Ocean Engineering 142 (2017) 411–418

Contents lists available at ScienceDirect

Ocean Engineering

journal homepage: www.elsevier.com/locate/oceaneng

Laboratory-scale investigation of the Ventilated-Trousers device acting as a suppressor of vortex-induced vibrations

M.M. Cicolin, G.R.S. Assi*

Department of Naval Architecture & Ocean Engineering, University of São Paulo, Brazil

ARTICLE INFO

Keywords:
Vortex-induced vibration
Suppression
Ventilated Trousers
Circular cylinders

ABSTRACT

Experiments have been carried out with circular cylinders fitted with a suppressor of vortex-induced vibrations called the *Ventilated Trousers* (VT). Tests were performed at laboratory scale in a free-surface water channel with fixed and free-to-respond models in one degree of freedom. The oscillating tests were performed with elastically mounted cylinders with low mass and damping ($m^*\zeta < 0.009$). Reynolds number varied from 5000 to 25000 and reduced velocity varied between 2 and 15. Tests with fixed models showed that the VT increased the mean drag and practically eliminated the fluctuating lift force when compared to a bare fixed cylinder. Free-response tests showed that the VT was able to reduce 60% of the peak amplitude of vibration, thus reducing the maximum drag compared with that of a bare oscillating cylinder. Three hypotheses are proposed to explain the physical mechanism underlying the suppression by the VT: local disruption of vortex shedding; three-dimensional disruption of the near wake; and the increase of hydrodynamic damping.

1. Introduction

The phenomenon of vortex-induced vibration (VIV) may be associated with serious damage caused to offshore cables, flexible pipes and other slender structures such as drilling risers. In the pursuit of viable solutions, the technological development of novel devices for suppressing VIV has been a current topic in both scientific and industrial communities. During the last three decades many devices have been investigated and offered as commercial products, such as helical strakes, fairings, shrouds, etc. However, following the industry demand for more efficient, robust and easy-to-install devices, new ideas for VIV suppressors are still under investigation. Helical strakes, for example, may be the most widely employed suppression device of them all. Strakes became sturdy contraptions with the improvement of molded plastic, but they still reduce VIV with the cost of increasing drag, taking considerable time to install and occupying large areas on the deck.

In this context, Brown and King (Brown, 2010) created an interesting new device for suppressing VIV of drilling risers called the "*Ventilated Trousers*", or simply VT in this paper. The VT is composed of a net of flexible cables through which an orthogonal array of bobbins (with a specific geometry) is fitted. In the words of its creators, the VT suppressor is "a loose fitting sleeve in the form of a light flexible net with integral bobbins in a special arrangement. It is omni-directional, rugged, and made from materials compatible with the offshore environment" (King et al., 2013). Essentially, the VT is an improvement on the idea of wrapping the drilling riser in a type of flexible cover able to deform with the flow and mitigate the body response to the hydrodynamic loads.

The suppression efficiency of the VT has been studied over the last years with promising results. Brown and King (2008), for example, performed experiments in a laboratory scale with flexible cylinders at $Re \approx 1.2 \times 10^6$, showing a 90% reduction of the VIV peak amplitude of displacement. (Reynolds number is defined as $Re = UD/\nu$, where U is the flow speed, D is the cylinder diameter and ν is the kinematic viscosity of water.) So far, all known experiments have been performed either with flexible pipes or near real conditions at sea, especially regarding the range of $3.7 \times 10^4 < Re < 1.2 \times 10^6$ and the structural properties of the risers (Brown and King, 2008; King et al., 2013).

1.1. Objective

Although these results are important for revealing the suppressing potential of the device, they do not shed much light on the physical mechanisms by which the VT is able to suppress vibrations. The present work is part of an investigation to study the interaction between model and flow at moderate Re and very low damping conditions. We are concerned with the scientific investigation of the hydrodynamic and hydroelastic mechanisms that make this type of suppressor effectively work.

This paper characterizes the VIV response of the VT in idealized

* Corresponding author.
E-mail address: g.assi@usp.br (G.R.S. Assi).

http://dx.doi.org/10.1016/j.oceaneng.2017.07.024
Received 30 August 2016; Received in revised form 10 May 2017; Accepted 5 July 2017

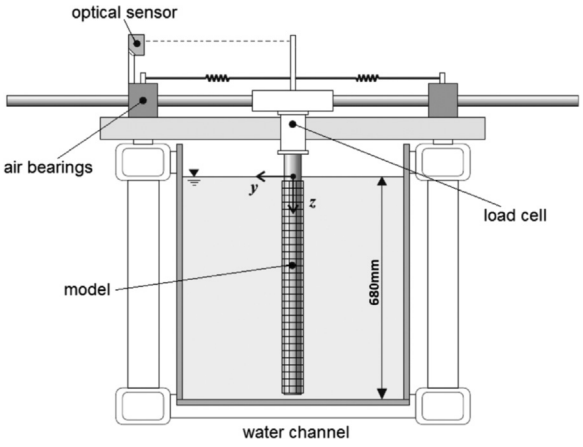

Fig. 1. Cross-section of the water channel showing the cylinder mounted on the elastic rig.

laboratory conditions, in which all variables were under control and crucial parameters were reduced to enhance response. The idea was to test the suppression device in the most pristine condition, indeed different from the real application in the ocean, but free from interference that could mask the understanding of the fundamental physical phenomena.

2. Experimental method

Experiments have been carried out in the free-surface water channel of NDF – Fluids and Dynamics Research Group – at the University of Sao Paulo, Brazil. The water channel has a test Section 0.7 m wide, 0.9 m deep and 7.5 m long. The flow speed U is variable up to 1 m/s, allowing for tests with different values of Reynolds number with a turbulence intensity less than 3%, obtained from velocity and turbulence profiles measured with hot-film anemometers by Assi (2005).

A rigid section of a circular cylinder was attached to a platform on a 1-degree-of-freedom rig, which allowed the model to oscillate freely in the transverse direction (y), as shown in a cross-sectional view in Fig. 1. The platform was mounted on air bearings to reduce friction, thus ensuring very low structural damping and maximum response. A pair of coil springs was responsible for providing the stiffness of the system and an optical positioning sensor (employing laser triangulation) measured the displacements with a resolution of 0.2 mm without adding extra damping.

A load cell installed between the cylinder and the platform measured instantaneous lift and drag forces acting on the cylinder. Because the load cell moved with the cylinder, the inertial component due to the mass of the model being accelerated was subtracted from the total force measured by the sensor. Details on the manufacturing and operation of the load cell were presented by Assi (2009). For further details on the elastic rig, other VIV experiments employing the rig and information on the facilities please refer to Cicolin et al. (2015, 2014) and Assi et al. (2013, 2010a, 2010b, 2009). Drag and lift coefficients have been reduced by dividing the fluid forces measured by the load cell by $\frac{1}{2}\rho U^2 DL$, where ρ is the specific mass of water, D is the external diameter and L is the submerged length of the cylinder.

Visualization of the flow in the near wake has been performed by the emission of hydrogen bubbles from a thin wire stretched parallel to the axis of the cylinder at about $1D$ upstream and $1D$ to the side of the centerline of the wake. A laser sheet illuminated a plane near the region where the free shear layers separated and rolled up to form vortices. A camera positioned perpendicular to the laser plane captured a field of view of almost $4D$ by $4D$ in the xz-plane.

The circular cylinder was cut from a perspex tube with an external diameter of D= 50 mm; the underwater aspect ratio was L/D = 13.4.

Table 1
Experimental parameters.

	m^*	$f_{N\,air}$ (Hz)	$f_N \equiv f_{N\,water}$ (Hz)	ζ_{air}	ζ_{water}
Bare cylinder	2.8	0.68	0.58	0.3%	1.6%
Cylinder with VT	2.9	0.66	0.56	0.3%	6.5%

The cylinder top end was attached to the load cell and the bottom end was closed to keep it watertight. Free-decay tests have been performed both in air and in water to determine the natural frequency and damping associated with the models. The natural frequencies were obtained from the power spectrum of displacement and the damping parameter from the logarithmic decrement of the decay response (values will be presented later when discussing the VIV response). Reduced mass m^* (defined as the ratio of total structural mas to the mass of displaced fluid) and structural damping ζ_{air} (defined as a fraction of the critical damping) were kept to a minimum in order to enhance the response. All experimental parameters are presented in Table 1.

The VT device was built with a flexible net of common polymeric twisted threads. Dozens of bobbins were manufactured out of polymeric rods, drilled through and attached to the net. All materials employed in the construction have been carefully chosen to ensure the VT was neutrally buoyant when submerged. Fig. 2 illustrates the assembly as it was ready for tests.

Some considerations must be presented concerning the geometric parameters of the VT model: The description found in the patent (Brown, 2010) allows for some variations on bobbin dimensions. The reference tests presented by Brown and King (2008), however, have been performed employing a fixed ratio between geometric variables. To allow for comparison, the same proportions for the bobbins, mesh size and bobbin distribution found in that report have been kept in the present work, as shown in Fig. 3. The mesh element width (w), net perimeter (p) and the ratio between the cylinder and the characteristic size of the bobbin (d/D) were specified.

Previously, Brown and King (2008) verified that a mesh element width of 5 times the bobbin characteristic dimension ($w = 5d$) resulted in a more effective VT than one in which $w = 3d$. They also reported that the net perimeter must be between $p = 4D$ and $\frac{3}{2}\pi D$ (or $4.71D$). Besides that, the patent recommended that the diameter ratio must vary between $d/D = 0.08$ and 0.125. Following this recipe and considering that the parameters are not completely independent, the largest possible mesh was built respecting the patent restrictions and recommendations. The final dimensions of the VT model employed in the present work are shown in Table 2.

3. Results

Preliminary experiments have been carried out with fixed models in flowing water in order to measure the hydrodynamic coefficients of drag (streamwise direction) and lift (cross-flow direction) acting on the cylinder with and without the VT. The mean drag coefficient ($\overline{C}_D$) obtained for the cylinder with and without VT are shown in Fig. 4(a). The bare cylinder presented $\overline{C}_D \approx 1.1$ for the whole range of Re, as expected and in agreement with Zdravkovich (1997). On the other hand, the VT increased $\overline{C}_D$ by approximately 25% when compared with that of a fixed bare cylinder, at least in the range $10 \times 10^3 < Re < 25 \times 10^3$. This result was expected, considering that the effective diameter of the cylinder with the VT is larger than the external diameter D of the bare cylinder, thus exposing a larger frontal area to the incoming flow. (Please note that $\overline{C}_D$ was normalized employing D for both cases.) But the main observation is that the complex geometry of the VT increased the loss of kinetic energy to the wake as the flow passed around the body, at least as far as fixed cylinders were concerned.

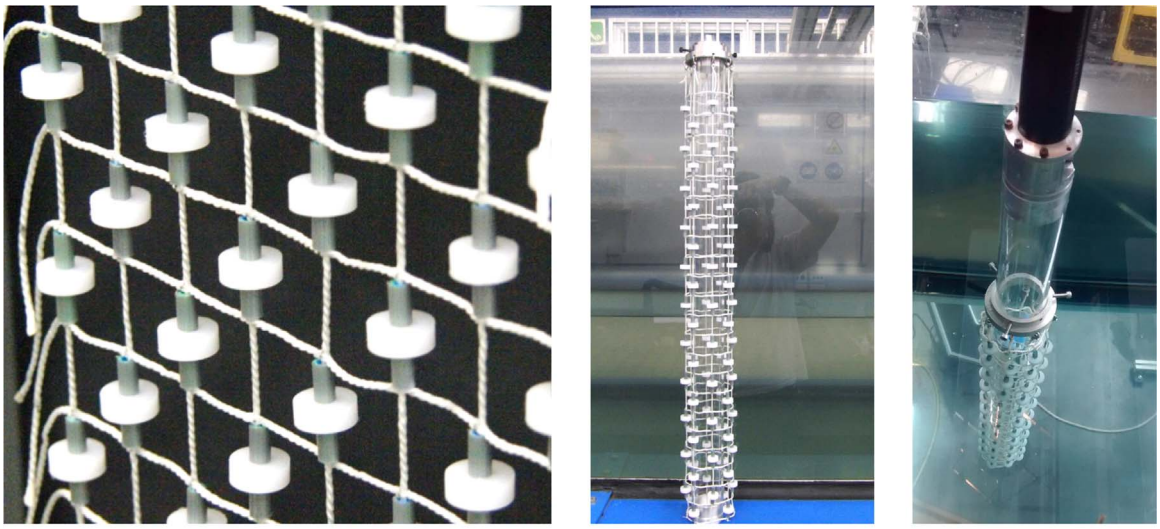

Fig. 2. (a) Details of the VT net with bobbins. (b) VT net fitted around the cylinder. (c) Cylinder with VT mounted on the rig and ready for tests in water.

Fig. 4(b) shows the magnitude of fluctuation of the lift force, calculated as the RMS of the lift signal. C'_L for a bare cylinder was near 0.2, showing considerable dispersion in this Re range. Norberg (2003) has already determined that such a dispersion occurs at this Re range due to the sensibility of the boundary conditions. Nevertheless, the results were in agreement with those obtained by Williamson (1996) for tests under similar conditions. In contrast with the increase in drag, the VT managed to almost completely reduce C'_L for the range of Re tested. This finding indicates that the VT indeed acts to considerably reduce the cyclic fluctuation of lift due to vortex shedding, at least for fixed cylinders.

The preliminary results obtained for the fixed cylinders do not guarantee that the VT will remain as effective in mitigating C'_L (and thus suppressing the force excitation) once the cylinder starts to oscillate. Previous studies have shown that three-dimensional suppressors that are effective in disrupting vortex shedding from fixed bodies, might not be so for oscillating bodies (for example, Kleissl and Georgakis, 2011; Owen et al., 2001; Bearman and Brankovic, 2004). Hence, experiments with free-to-responde models were necessary to evaluate the behavior of the VT while responding to VIV.

3.1. Cross-flow VIV

Free-to-respond experiments have been performed with cylinders with and without the VT in the same range of Re as in the fixed tests. The objective was to characterize the cross-flow VIV response of the cylinder with VT compared to that of the bare cylinder. The pair of springs (setting the natural frequency f_N of the system) was chosen to ensure that the whole synchronization range of VIV fitted within the Re range of the experiment. As mentioned before, m^* and ζ_{air} were kept to a minimum in order to enhance the response.

Table 2
Model parameters.

Cylinder diameter	D	50 mm	
Bobbin characteristic dimension	d	5.8 mm	$0.11D$
Mesh element width	w	29 mm	$5d$
Net perimeter	p	232 mm	$4.64D$
Submerged length	L	670 mm	$13.4D$
VT dry mass		161 g	

Fig. 5 presents the VIV response of the cylinder with VT compared to that of a bare cylinder for a wide range of reduced velocity (U/Df_N). The non-dimensional amplitude of vibration $\hat{y}/D$ (top plot) was obtained by multiplying the RMS of the displacement signal by $\sqrt{2}$, thus yielding the equivalent amplitude of a harmonic oscillation. The non-dimensional dominant frequency of oscillation f/f_N (bottom plot) was obtained by applying a fast Fourier transform on the displacement

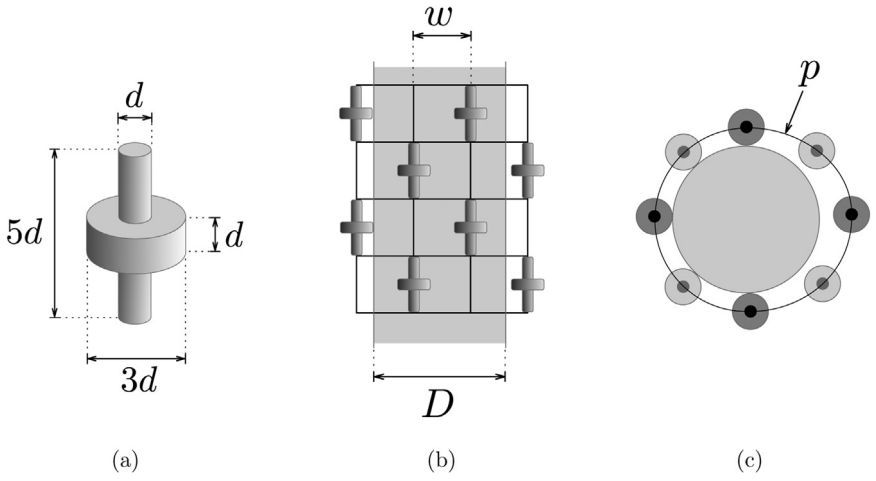

Fig. 3. Geometric properties of the VT suppressor: (a) bobbin dimensions (b) mesh arrangement and (c) cross-section view of the model.

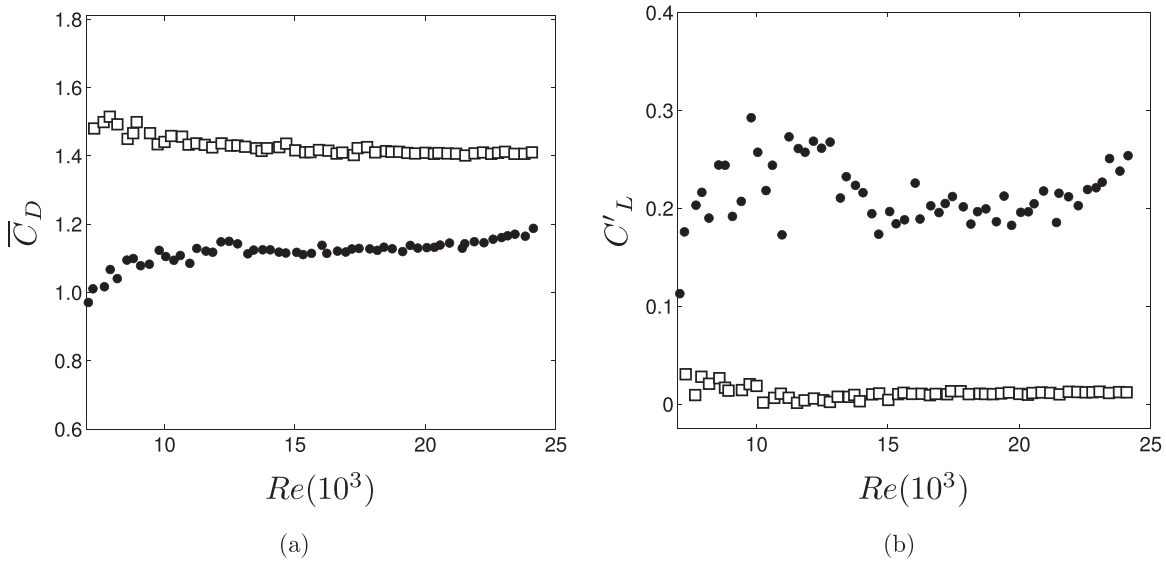

Fig. 4. Force coefficients for fixed models versus *Re*: (a) mean drag and (b) RMS of fluctuating lift. Key: •bare cylinder, □ cylinder with VT.

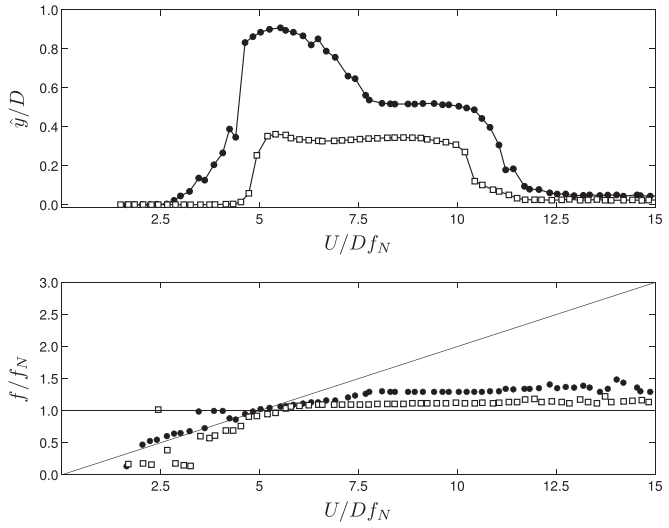

Fig. 5. Displacement (top) and frequency (bottom) responses versus reduced velocity for the cylinders under VIV. Key: •bare cylinder, □ cylinder with VT.

data. (Please remind that f_N was determined for the cylinder immersed in water.)

The bare cylinder presented a typical VIV response, in agreement with the results obtained by Williamson and Govardhan (2004). The peak response amplitude occurred at $U/Df_N \approx 5$, when the frequency of vortex shedding resonated with the natural frequency of the system. At around this point, f/f_N crossed the line representing $f/f_N = 1$ and remained close to the natural frequency of the system until the end of the synchronization range. For $U/Df_N > 12$ the response died out, marking the end of the VIV synchronization range. Please note that a residual vibration of insignificant amplitude and frequency near to the natural frequency remained for higher reduced velocities (higher *Re*) due to turbulence buffeting.

At first sight, it is evident that the cylinder with the VT presents a suppressed response when compared to that of a bare cylinder. One may note that the displacement response curve for the VT actually "fits inside" the typical VIV curve for the bare cylinder, thus showing a reduced amplitude and synchronization range. The upper and lower branches of vibration, clearly identified for the bare cylinder, have now disappeared with the VT. A reminiscence of the upper branch still holds the peak amplitude of vibration at $\hat{y}/D \approx 0.4$ close to $U/Df_N = 5.5$, resulting in a 60% reduction when compared with that of the bare cylinder. Interestingly the frequency signature of the cylinder with the VT is fairly similar to that of the bare cylinder, except for small variations due to differences in $f_{N\,water}$ of both systems.

Fig. 6 compares examples of the time series of displacement for roughly 60 cycles of vibration (t is time) for a bare cylinder and a cylinder with VT during the VIV synchronization range. It becomes clear that both responses are indeed harmonic, each with a distinct dominant frequency for the entire sample. At $U/Df_N = 6$, in which the bare cylinder oscillated in the upper branch of response, the maximum y/D of the cylinder with VT was not only less than half of that of the bare cylinder, but also the envelope of displacement presented less variations in time. At $U/Df_N = 9$, near the end of the synchronization range, both envelopes became equally well behaved.

Drag measurements obtained during the VIV experiments are shown in Fig. 7(a). As expected, the mean drag coefficient of the bare cylinder increased significantly during the synchronization range, reaching $\overline{C}_D \approx 3$ when the cylinder oscillated with the largest displacement. As the amplitude decreased towards the end of synchronization,

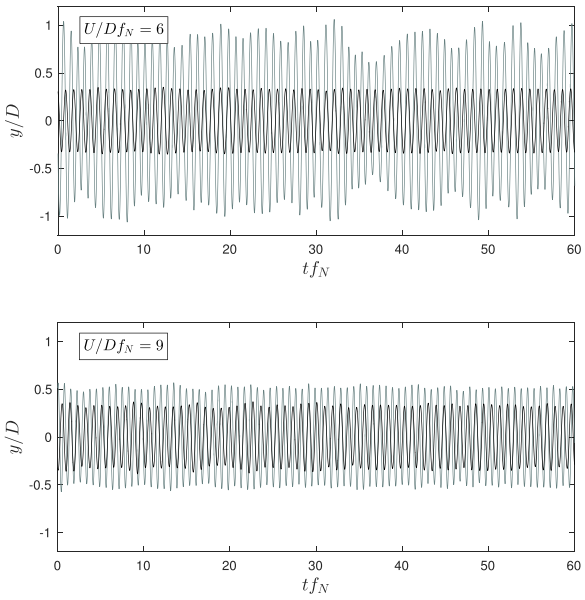

Fig. 6. Examples of time series of displacement during the VIV response for a bare cylinder (gray line) and a cylinder with VT (black line).

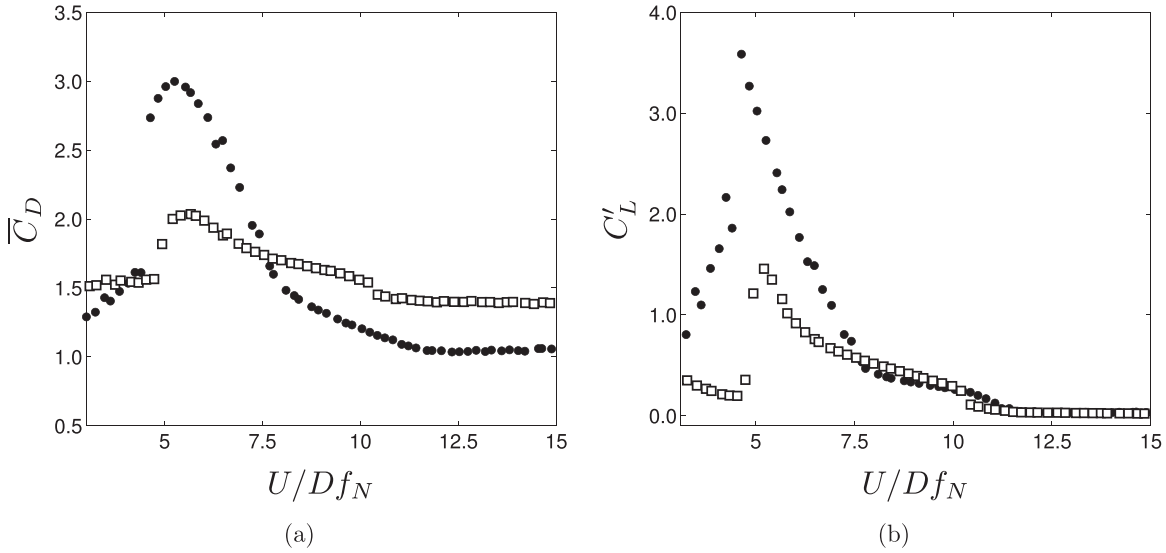

Fig. 7. (a) Mean drag and (b) RMS of lift coefficients versus reduced velocity for the cylinders under VIV. Key: • bare cylinder, □ cylinder with VT.

drag was restored to $\overline{C}_D \approx 1$, very close to the value found for the fixed cylinder. These results are in good agreement with those obtained by Williamson (1996) for similar tests. The cylinder with the VT showed the same behavior, presenting a maximum value when the displacement amplitude was the largest, then decreasing as the amplitude became smaller until it reached the value measured for a fixed cylinder with VT for $U/Df_N > 12$. It is worth noting that the maximum value of $\overline{C}_D \approx 2$ was almost 30% lower than that found for the bare cylinder. But after the synchronization range, $\overline{C}_D$ approximated to 1.4, which was practically the same value found for the fixed model, but larger than the $\overline{C}_D$ of a bare cylinder.

RMS of lift coefficient presented in Fig. 7(b) shows that C'_L of a bare cylinder increased up to approximately 3.7 during VIV resonance, at $U/Df_N \approx 5$, when there was maximum energy transfer from the flow to the system. As the reduced velocity increased, C'_L decreased reaching values close to zero when the synchronization ended. As expected, there was a strong relationship between C'_L and $\hat{y}/D$, as explained by Williamson (1996). The RMS of lift coefficient of the cylinder with the VT followed a similar trend as that for the bare cylinder, but with values significantly lower. A maximum value of $C'_L \approx 1.5$ was only 40% of that of the bare cylinder, showing that the VT is capable of reducing, to a certain extent, the magnitude of the fluctuating force exciting the cylinder also during VIV.

A detailed view of the frequency signature of the phenomenon is presented in Fig. 8. The top plot presents the VIV response as a reference. The middle plot presents color contours representing the power spectrum of displacement, highlighting the dominant frequencies (f/f_N) versus reduced velocity. The bottom plot, presents a similar power spectrum, this time for the lift force acting on the body, in which the dominant frequency of lift (f_{C_L}/f_N) is noticeable. The highest peak in the spectrum for each reduced velocity resulted in the points plotted before in Fig. 5. Refer to Assi (2009) for details on how these plots have been made.

The f/f_N spectrum for the bare cylinder (Fig. 8(a)) shows the typical frequency signature for the VIV response. A single branch of dominant frequency remained near the natural frequency of the system during the lock-in range. Both displacement and lift showed the same signature, as expected. After the end of lock-in, for $U/Df_N > 12$, the cylinder presented minute vibrations due to turbulence buffeting and f_{C_L}/f_N followed the $St = 0.2$ line (indicated by the inclined solid line on the plot).

The frequency signature for the cylinder with VT (Fig. 8(b)) was essentially the same, with a single frequency branch dominating along the synchronization range. However, outside the lock-in range, we did not see a significant component of f_{C_L}/f_N following the $St = 0.2$ (not even when the flow was more energetic at $U/Df_N > 12$), but a broader lift spectrum instead. This explains the lower values of C'_L measured for a fixed cylinder and presented before in Fig. 4(b). While the three-dimensional geometry of the VT might be efficient in disrupting vortex shedding from fixed cylinders, a coherent wake may reappear as the cylinder is excited into cross-flow oscillations near its natural frequency.

4. Discussion on the hydrodynamic mechanisms

The preliminary tests with fixed models revealed important features of the behavior of the VT suppressor. The increase in mean drag was not a surprise, since the installation of the VT around the cylinder simply increases the effective frontal area facing the incoming flow. The complex geometry of the net and bobbins also increased the surface area of the system, resulting in stronger separated flow around the net and bobbins as well as increased friction losses.

In another recent work (Cicolin and Assi, 2017) we have observed that the VT increases the vortex-formation length in the near wake. We argued that "the longer formation length found for the VT is responsible for a decrease in the fluctuating lift feeding back to excite the cylinder into VIV." Particle-image velocimetry (PIV) measurements of the wake, reproduced here in Fig. 9, reveled that "while most of the flow is separated from the outer surfaces of the bobbins, the entrainment of flow that permeates the VT mesh bleeds through to feed the near wake region, extending the vortex-formation length and increasing the base pressure." This mechanism, which interferes with the two-dimensional formation of vortices, was attributed to the peculiar geometry of the bobbins working like a shroud.

On the other hand, it was rather unexpected that the VT managed to reduce the RMS of lift to almost zero for the whole range of Re, hence we conclude that the VT successfully acted to weaken the vortex-excitation force. Considering that hydrodynamic loads were measured as an integral force at the top of cylinder, it is reasonable to hypothesize that the VT could either eliminate the sectional lift force, or uncorrelate it along the span of the cylinder. This is a clear indication that the three-dimensional geometry of the VT suppressor is important for its effectiveness.

In order to investigate three-dimensional flow structures along the span, flow visualization employing hydrogen bubbles has been performed for a fixed cylinder with and without VT at Re=7800. A curtain of bubbles was released from a thin wire and illuminated by a laser sheet on the xz-plane, parallel to the axis of the cylinder. Figs. 10–12

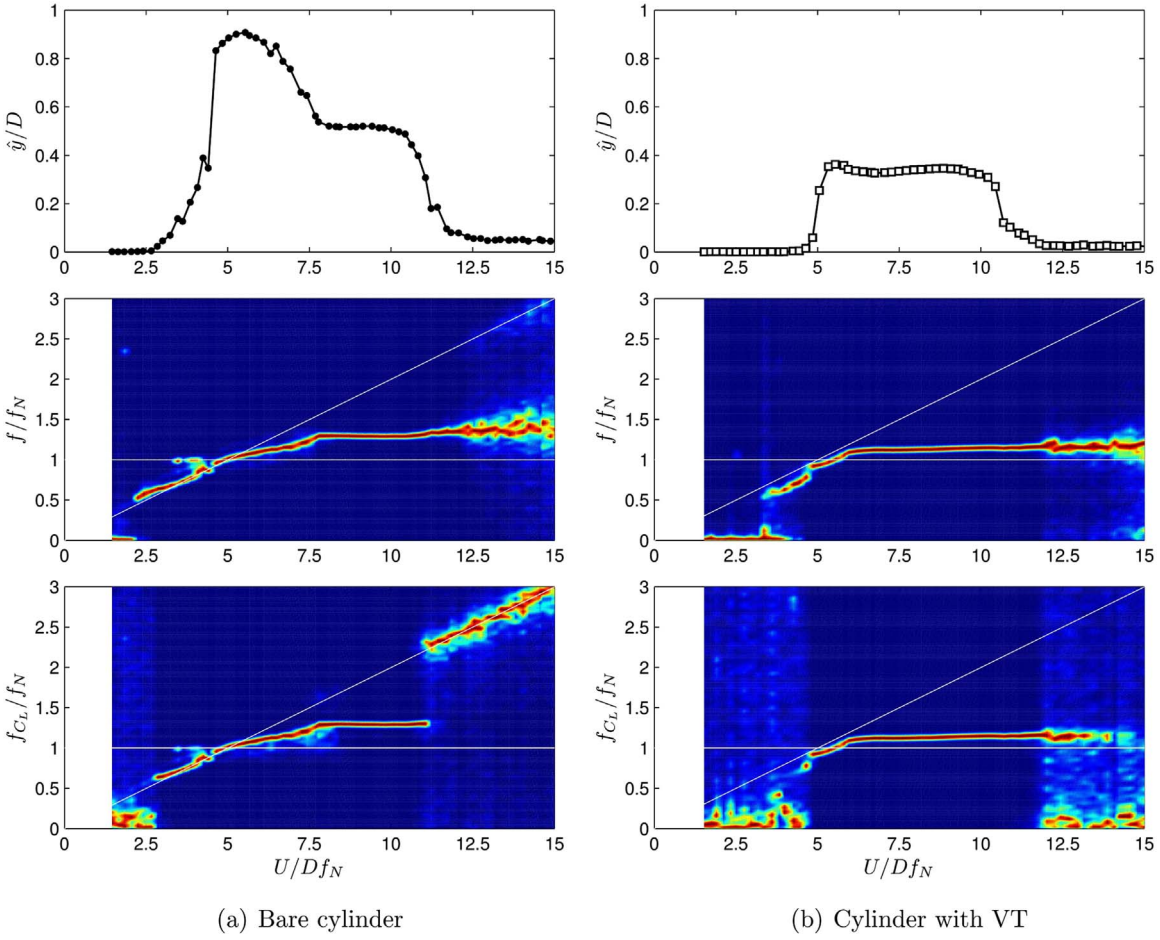

Fig. 8. Amplitude of displacement (top) and power spectra of displacement (middle) and lift (bottom) for both models.

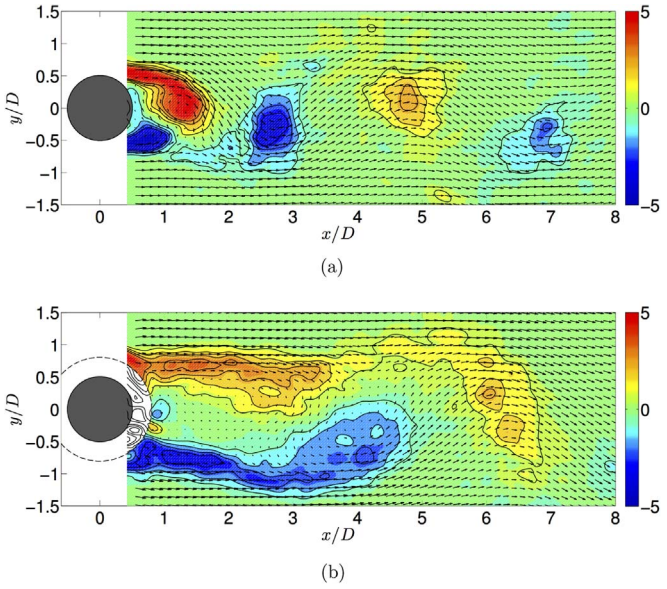

Fig. 9. Phase-averaged vorticity contours (s^{-1}) in the near wake of (a) a bare cylinder and (b) a cylinder with VT. *Re*=9000. Reproduced from Cicolin and Assi (2017).

compare the three-dimensional wake structures along the span created by the VT with that of a bare cylinder.

Fig. 10 presents two examples of the three-dimensional wake structure downstream of a bare cylinder (the cylinder walls are represented by thick lines, while the center is marked by a dot-dashed line). A clear vortex filament parallel to the axis of the cylinder is seen at its maximum extension. The estimated vortex-formation length is seen to be around 1*D* and 2*D* downstream of the cylinder center, which is in good agreement with other values found in the literature for this *Re* range, including the value of 1.5 measured by Cicolin and Assi (2017) for *Re*=9000 and reproduced in Fig. 9.

The flow structures in the wake of a cylinder with VT are shown in Fig. 11. Distinct three-dimensionalities associate with the bobbins are visible in the near wake, specially for the first 2*D* downstream of the cylinder center. The formation of a coherent vortex filament is not seen to be occurring within the plane illuminated by the laser sheet, which agrees with Cicolin and Assi (2017), who measured a vortex-formation length of 5.31 for *Re*=9000 (Fig. 9(b)). A detailed view of the flow around the VT is seen in Fig. 12, confirming that complex three-dimensional flow structures generated at the scale of the bobbins dominate the flow in the near wake. We believe these flow structures enhance flow entrainment and mixing of the free shear layers, disrupting the formation of an organized vortex wake.

In essence, we believe that (i) the shrouding effect acting on the two-dimensional level proposed by Cicolin and Assi (2017) combined with (ii) the three-dimensional disruption of the near wake by the bobbins are the hydrodynamic mechanisms that weaken the vortex-shedding excitation force that drives VIV.

Nevertheless, other secondary effects might also be playing a role in reducing the response of a cylinder with VT. The decay tests performed in air and in water raised another important aspect associated with the VIV response. Although both cylinders were designed to present the same level of structural damping (ζ_{air}), the VT increased the hydrodynamic damping of the system when submerged: ζ_{water} for the cylinder with VT is almost 5 times higher than that of the bare cylinder. This is due to the viscous loss of energy as the cylinder oscillates in still

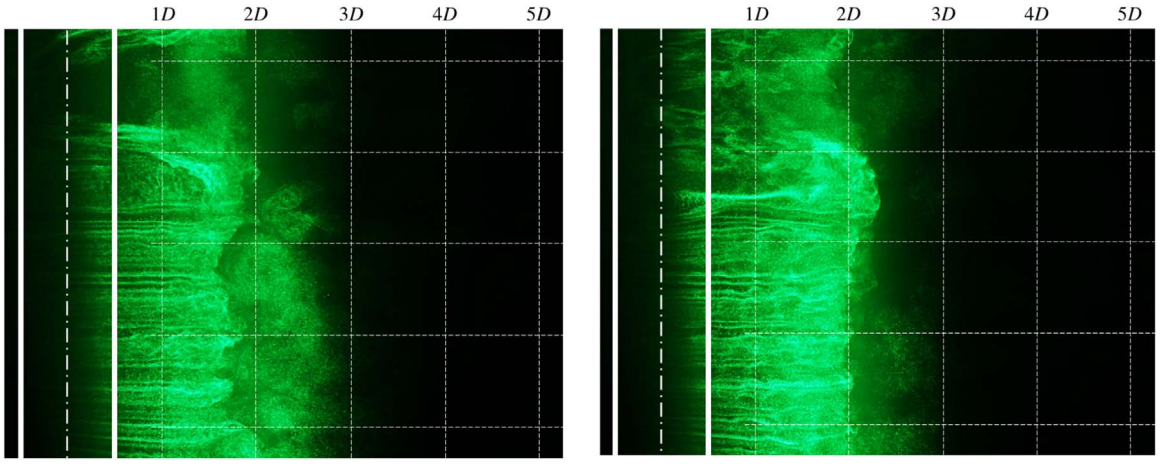

Fig. 10. Visualization of the near wake of a fixed bare cylinder. Two instants. Flow is from left to right. *Re*=7800.

water. Of course the interaction of the oscillating cylinder with its own wake will change its perception of the fluid loads (Vandiver, 2012, refer to), yet it is reasonable to think that the VT is likely to present lower amplitudes of vibration due to its increased non-linear hydrodynamic damping. A considerable number of works (Vikestad et al., 2000; Blevins, 2001, for example) show that the VIV response is very sensitive to damping, especially at low mas ratios.

Consequently, we believe that the suppression efficiency of the VT in real applications out in the ocean may be higher than that observed in this laboratory experiment performed in idealized conditions with low mass and damping. In real conditions at sea, structural damping reaches values ten times higher, while hydrodynamic damping may also be increased due to higher-*Re* and higher-turbulence effects. In spite of increasing drag for non-oscillating models, the VT reduces drag when the maximum amplitude of vibration occurs. All facts combined make the VT an attractive solution as far as hydroelasticity is concerned (not to mention other criteria regarding storage and installation).

5. Conclusion

The cross-flow VIV response of a cylinder with VT was characterized through the synchronization range for $Re=2 \times 10^3$ to 25×10^3 and reduced velocities up to 15. Our main conclusion in the present work is that the VT suppressor is capable of reducing the VIV peak amplitude of displacement in 60%, with an increase of about 25% in drag, when compared to a bare cylinder under VIV. This was achieved for idealized conditions in the laboratory: at moderate Reynolds number, low mass ratio and extremely low-damping systems.

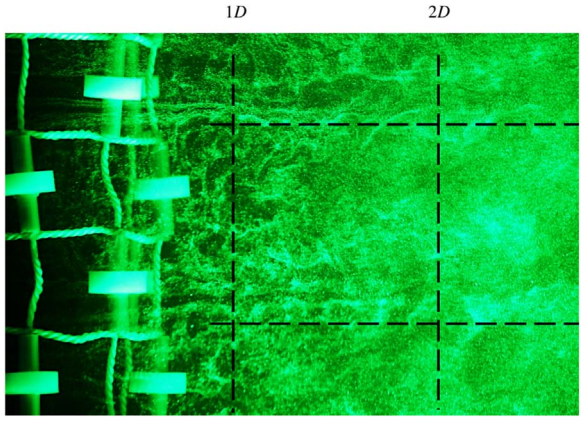

Fig. 12. Detail of the flow structures around the VT. Flow is from left to right. *Re*=7800.

Experiments with fixed models also confirmed that a cylinder with VT presents reduced RMS of lift, but increased drag when compared to a bare cylinder. While the three-dimensional geometry of the VT might be efficient in disrupting vortex shedding from fixed cylinders, a coherent wake may reappear as the cylinder is excited into cross-flow oscillations. Only a small lift force is required for that to occur with low-mass-damping systems under VIV.

Results helped us raise three hypotheses to explain the physical mechanism underlying the suppression by the VT: (i) local disruption of the two-dimensional vortex shedding mechanism and the formation of the wake; (ii) global changes in the three-dimensional flow structure

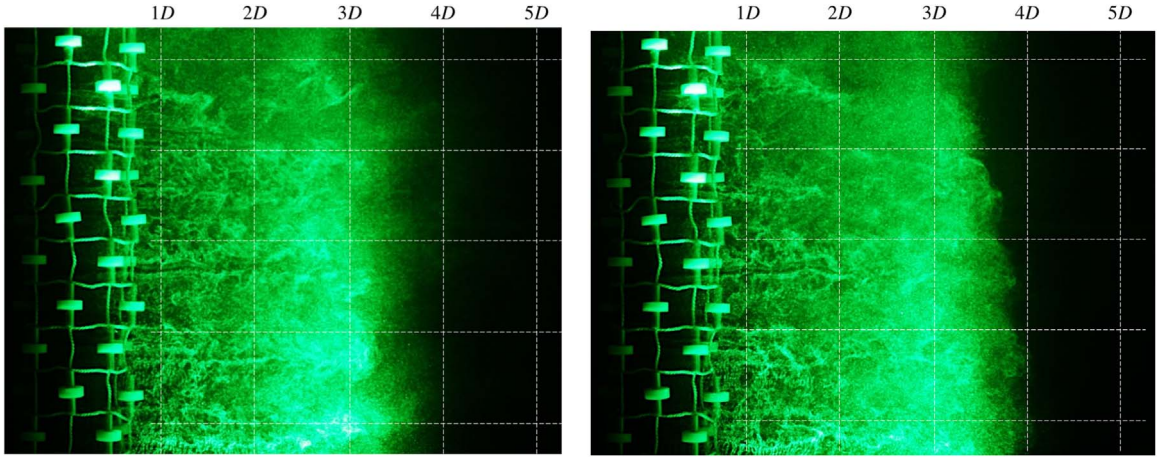

Fig. 11. Visualization of the near wake of a fixed cylinder with VT. Two instants. Flow is from left to right. *Re*=7800.

along the span of the cylinder caused by the flow around the bobbins; and (iii) the increase of hydrodynamic damping caused by the VT. Future works should try to isolate parameters to verify whether one or a combination of mechanisms is responsible for the suppression.

Finally, we would like to highlight that idealized experiments in laboratory scale are designed to allow for the control of the fundamental parameters involved in the investigation, thus shedding light on the physical mechanisms being studied. We cannot fully predict how the VT would behave in real applications at much larger scales. We can make reasonable assumptions knowing that Reynolds number, turbulence intensity, structural damping and other parameters will be significantly different. Data collected from large-scale field tests cannot be directly compared to the results presented in this paper without such considerations being made.

Acknowledgements

MM Cicolin is thankful to the support of ANP Brazilian Agency of Petroleum, Natural Gas and Biofuels. GRS Assi is grateful to FAPESP (2011/00205-6, 2014/50279-4), CNPq (306917/2015-7) and the Brazilian Navy.

References

Assi, G.R.S., 2005. Experimental Study of the Flow Interference Effect around Aligned Cylinders (Master's thesis). University of São Paulo, São Paulo, Brazil, (in portuguese) Available from:www.teses.usp.br.

Assi, G.R.S., 2009. Mechanisms for Flow-induced Vibration of Interfering Bluff Bodies (Phd thesis). Imperial College London, Available from: ⟨www.ndf.poli.usp.br/~gassi⟩.

Assi, G.R.S., Bearman, P.W., Carmo, B.S., Meneghini, J.R., Sherwin, S.J., Willden, R.H.J., 2013. The role of wake stiffness on the wake-induced vibration of the downstream cylinder of a tandem pair. J. Fluid Mech. 718, 210–245, (3).

Assi, G.R.S., Bearman, P.W., Kitney, N., 2009. Low drag solutions for suppressing vortex-induced vibration of circular cylinders. J. Fluids Struct. 25, 666–675.

Assi, G.R.S., Bearman, P.W., Kitney, N., Tognarelli, M.A., 2010a. Suppression of wake-induced vibration of tandem cylinders with free-to-rotate control plates. J. Fluids Struct. 26, 1045–1057.

Assi, G.R.S., Bearman, P.W., Meneghini, J.R., 2010b. On the wake-induced vibration of tandem circular cylinders: the vortex interaction excitation mechanism. J. Fluid Mech. 661, 365–401, (10).

Bearman, P.W., Brankovic, M., 2004. Experimental studies of passive control of vortex-induced vibration. Eur. J. Mech.- B/Fluids 23 (1), 9–15.

Blevins, R.D., 2001. Flow-Induced Vibration 2nd Ed.. Krieger Publishing Company.

Brown, A., 2010. Device and Method for Suppressing Vortex-induced Vibrations. Tech. rep., United States Patent Application Publication.

Brown, A., King, R., 2008. Tests with flexible quasi-fairing to reduce riser drag, suppress viv and limit drilling down-time. In: Proceedings of the Offshore Technology Conference (OTC 2008). p. 19161.

Cicolin, M.M., Assi, G.R.S., 2017. Experiments with flexible shrouds to reduce the vortex-induced vibration of a cylinder with low mass and damping. Appl. Ocean Res. 65, 290–301.

Cicolin, M.M., Freire, C.M., Assi, G.R.S., 2014. Suppression of the vortex-induced vibration of a circular cylinder with permeable meshes. In: Proceedings of the 4th Joint US-European Fluids Engineering Summer Meeting.

Cicolin, M.M., Freire, C.M., Assi, G.R.S., 2015. VIV response and drag measurements of circular cylinders fitted with permeable meshes. In: Proceedings of the 34th International Conference on Ocean, Offshore and Arctic Engineering.

King, R., Brown, A., Braaten, H., Russo, M., Baarholm, R., Lie, H., 2013. Suppressinf full scale riser viv with the vt suppressor. In: of Mechanical Engineers (ASME), A.S. (Ed.), Proceedings of the 32th International Conference on Ocean, Offshore and Arctic Engineering (OMAE 2008). p. 11642.

Kleissl, K., Georgakis, C., 2011. Aerodynamic control of bridge cables through shape modification: A preliminary study. J. Fluids Struct. 27 (7), 1006–1020.

Norberg, C., 2003. Fluctuating lift on a circular cylinders: Review and new measurements. J. Fluids Struct. 17, 57–96.

Owen, J.C., Bearman, P.W., Szewczyk, A.A., 2001. Passive control of VIV with drag reduction. J. Fluids Struct. 15, 597–605.

Vandiver, J.K., 2012. Damping parameters for flow-induced vibration. J. Fluids Struct. 35, 105–119.

Vikestad, K., Larsen, C.M., Vandiver, J.K., 2000. Norwegian deepwater program: damping of vortex-induced vibrations. In: Proceedings of the Offshore Technology Conference. No. OTC 11998.

Williamson, C., 1996. Three-dimensional wake transition. J. Fluid Mech. 328, 345–407.

Williamson, C., Govardhan, R., 2004. Vortex-induced vibrations. Annu. Rev. Fluid Mech. 36, 413–455.

Zdravkovich, M., 1997. Flow Around Circular Cylinders: Vol.1 – Fundamentals 1st Ed.. Oxford Science Publications.